Tellus SERIES A DYNAMIC METEOROLOGY AND OCEANOGRAPHY
PUBLISHED BY THE INTERNATIONAL METEOROLOGICAL INSTITUTE IN STOCKHOLM

A simple model of ocean temperature re-emergence and variability

By PETER KOWALSKI[1]* and MICHAEL DAVEY[2,3], [1]*Department of Mathematics, University College, London, UK*; [2]*Met Office, Exeter, UK*; [3]*Centre for Mathematical Sciences, University of Cambridge, Cambridge, UK*

(Manuscript received 26 May 2015; in final form 15 October 2015)

ABSTRACT

A simple stochastic one-dimensional model of interannual mid-latitude sea surface temperature (SST) variability that can be solved analytically is developed. A novel two-season approach is adopted, with the annual cycle divided into two seasons denoted summer and winter. Within each season the mixed layer depth is constant, and the transition of the mixed layer from summer to winter and vice versa is discontinuous. SST anomalies are forced by random atmospheric heat fluxes, assumed to be constant within each season for simplicity, with linear damping to represent atmospheric feedback. At the start of summer the initial SST anomaly is set equal to that at the end of the previous winter, and at the start of winter the initial temperature anomaly is found by instantaneously mixing the summer mixed layer with the heat stored below in the deeper winter mixed layer, thereby explicitly taking into account the 're-emergence mechanism'. Two simple auto-regressive equations for the summer and winter SST anomalies are obtained that can be easily solved. Model parameters include seasonal damping coefficients, mixed layer depths and standard deviations of the atmospheric forcing. Analytic expressions for season-to-season correlation and variability and power spectra are used to explore and illustrate the effects of the parameters quantitatively. Among the results it is found that, with regard to winter-to-winter temperature correlation, the re-emergence pathway is more influential than persistence via the summer mixed layer when the winter layer is more than twice the depth of the summer layer. With regard to winter temperature variability, the effect of a deeper winter mixed layer is to decrease the sensitivity to surface forcing and thus decrease variability, but also to increase persistence via re-emergence and thus increase variance at multidecadal scales.

Keywords: re-emergence, ocean temperature variability, mixed layer

1. Introduction

Namias and Born (1970, 1974) described a tendency for sea surface temperature (SST) anomalies to recur from one winter to the next without persisting in the intervening summer in the North Pacific and North Atlantic oceans. They hypothesised that the nature of this recurrence is closely tied to the seasonal mixed layer cycle. In the winter, upper ocean temperature anomalies are created in a deep mixed layer and then sequestered below the mixed layer as it shoals in the following spring and summer, sheltered from the summer surface heat fluxes. The summer SST anomalies are altered by the summer surface heat fluxes, subsequently losing their relationship with SST anomalies formed at the end of the previous winter. When the mixed layer deepens in the following late autumn and early winter, portions of these preceding winter temperature anomalies are re-entrained into the winter mixed layer, subsequently impacting the SST. Alexander and Deser (1995) investigated this theory of Namias and Born further using observational data taken from ocean weather ships in the North Atlantic and North Pacific oceans, and established a significant statistical link between subsurface temperature anomalies and SST anomalies from preceding and subsequent winter seasons. They termed the theory of Namias and Born 'the re-emergence mechanism'. The type of re-emergence investigated by Namias and Born (1970, 1974) and Alexander and Deser (1995) is termed 'local'; re-emergence occurs at the same location where SST anomalies were formed in the previous winter. Since the work of Alexander and Deser (1995), further evidence for local re-emergence in the North Atlantic (Watanabe and Kimoto,

*Corresponding author.
email: p.kowalski@ucl.ac.uk

Citation: Tellus A 2015, **67**, 28651, http://dx.doi.org/10.3402/tellusa.v67.28651

2000; Timlin et al., 2002; Deser et al., 2003; Hanawa and Sugimoto, 2004) and North Pacific (Alexander et al., 1999; Deser et al., 2003; Hanawa and Sugimoto, 2004) has been obtained. More recently, Ciasto and Thompson (2009) have presented observational evidence for re-emergence in the extratropical Southern Hemisphere. The focus of the present study is local re-emergence.

The influence of re-emergence on mid-latitude SSTs is highly relevant to seasonal prediction. Rodwell and Folland (2002) demonstrated that through re-emergence a pre-season North Atlantic SST pattern is a significant predictor for the winter North Atlantic Oscillation (NAO) index, and this work was extended by Folland et al. (2012). The relation of late winter 2009/10 North Atlantic SST to early winter 2010/11 SST through re-emergence, and hence on the NAO, is described in detail in Taws et al. (2011).

A commonly used measure of local re-emergence is the auto-correlation function (ACF) of the observed local SST (Alexander et al., 1999; Watanabe and Kimoto, 2000; Timlin et al., 2002; Deser et al., 2003; De Coëtlogon and Frankignoul, 2003; Hanawa and Sugimoto, 2004). If the winter-to-preceding-winter value of the ACF is larger than the winter-to-preceding-summer value, then re-emergence is likely to be influencing the winter SST. Key factors that influence the magnitude of winter-to-preceding winter and winter-to-preceding summer values of the ACF are:

- The size of the mean winter mixed layer depth (e.g. Timlin et al., 2002; Deser et al., 2003); shallower mean winter mixed layers have a smaller heat capacity and thus subsurface temperature anomalies are less likely to have an influence on the SST in subsequent winter seasons through the entrainment process. The statistical signature of the re-emergence mechanism is therefore stronger in oceans associated with large mean winter mixed layers, such as the North Atlantic (e.g. Deser et al., 2003).
- The difference between the mean summer and winter mixed layer depths; re-emergence dominates the winter temperature in regions where the mean winter mixed layer is much larger than the mean summer mixed layer (Timlin et al., 2002; Hanawa and Sugimoto, 2004).
- Atmospheric feedback, which controls the rate at which SST anomalies are damped by the overlying atmosphere; stronger feedback reduces the persistence of SST anomalies (Ciasto et al., 2010).
- The size of the winter net surface heat flux variations; if these are large then winter SST variability will be dominated by these, with less re-emergence effects (Zhao and Li, 2012).

These basic factors and processes can be represented by the following simple bulk mixed-layer model introduced by Deser et al. (2003):

$$h\frac{dT'}{dt} = \frac{F'}{\rho_0 c_p} - \frac{\kappa}{\rho_0 c_p}T' - \mathcal{H}(\frac{dh}{dt})\frac{dh}{dt}(T' - T'_b), \qquad (1)$$

where ρ_0 is the characteristic density of the ocean, c_p the specific heat capacity at constant pressure, $h(t)$ is a fixed seasonal mixed layer depth cycle, $T'(t)$ the temperature anomaly (constant throughout the mixed layer), $T'_b(t)$ the temperature anomaly just below the mixed layer, $\kappa(t)$ the atmospheric damping coefficient with a fixed seasonal cycle, and F' the stochastic atmospheric forcing typically modelled as Gaussian white noise that varies interannually as well as within the seasonal cycle. The Heaviside step function $\mathcal{H}$ term is zero if the mixed layer is steady or shoaling and 1 if the mixed layer is deepening. Equation (1) can be viewed as an extension to the classical climate noise paradigm of Frankignoul and Hasselmann (1977). Deser et al. (2003) demonstrated that the simulated ACFs of the North Pacific and North Atlantic, which were calculated using model SST data from eq. (1), were favourable fits to the corresponding observed ACFs, and subsequently proposed that eq. (1) forms the basis for understanding the persistence of mid-latitude SST anomalies.

In this paper, a version of eq. (1) is presented, simplified to the point that statistical relations such as the ACF can be obtained analytically. In Section 2, the simple two-season stochastic model of the re-emergence mechanism is derived. In Sections 3 and 4, we investigate and quantify the effects of varying model parameters on the winter-to-winter temperature correlation and the winter temperature variance. In Section 5, the power spectrum of the winter temperature is obtained analytically in terms of model parameters, and explored. Summer-to-winter statistics are described in Section 6, and some measures of re-emergence are discussed in Section 7. Summer-to-summer statistics are discussed briefly in Section 8.

2. The stochastic two-season auto-regressive model

The key simplification is to represent the seasonal cycle by two six-month seasons, summer and winter (denoted by subscripts S and W, respectively) in each year i. Thus the sequence is winter i − 1 → summer i → winter i …. The mixed layer depths h_S and h_W remain constant within each season, so from eq. (1) the mixed layer temperature variations within each season are governed by

$$\frac{dT_S}{dt} = \frac{Q_S}{\rho_0 c_p h_S} - \frac{\kappa_S}{\rho_0 c_p h_S}T_S, \qquad (2)$$

$$\frac{dT_W}{dt} = \frac{Q_W}{\rho_0 c_p h_W} - \frac{\kappa_W}{\rho_0 c_p h_W} T_W. \tag{3}$$

The damping coefficients κ_S and κ_W are taken as constant in each season. The heat fluxes Q_S and Q_W are also taken to be constant within each season, and as such they represent the net effect of fluxes that fluctuate throughout each season on shorter 'weather' timescales. Interannual variations of Q_S and Q_W are modelled as uncorrelated random variables, so future atmospheric conditions are independent of those in the preceding seasons. Formally,

$$Q_W \sim \sigma_{QW} \mathcal{N}(0,1), \tag{4}$$

$$Q_S \sim \sigma_{QS} \mathcal{N}(0,1), \tag{5}$$

where $\mathcal{N}(0,1)$ is a normal random variable with mean zero and unit standard deviation, and σ_{QW} and σ_{QS} are the standard deviations of the summer and winter atmospheric forcing, respectively.

2.1. Transition relations

Denote the years by a subscript i, and the summer and subsequent winter of year i by the subscripts Si and Wi, respectively. At the start of summer in year i, the initial temperature anomaly T_{si0} is set equal to the anomaly T_{Wi-1} at the end of the previous winter:

$$T_{Si0} = T_{Wi-1}. \tag{6}$$

The temperature anomaly T_{Wi0} at the start of winter in year i is found by instantaneously mixing the summer mixed layer and the sequestered winter layer heat content:

$$\rho_0 c_p h_W T_{Wi0} = \rho_0 c_p h_S T_{Si} + \rho_0 c_p (h_W - h_S) T_{Wi-1}, \tag{7}$$

where T_{Si} denotes the end-of-summer temperature anomaly. Thus

$$T_{Wi0} = r T_{Si} + (1-r) T_{Wi-1}, \tag{8}$$

where

$$r = h_S / h_W \tag{9}$$

is the ratio of the summer and winter mixed layer depths, with $r \le 1$.

The term $(1-r)T_{Wi-1}$ contains the re-emergence mechanism, and to help monitor its effect in various circumstances we introduce a 'process flag' parameter γ in eq. (8), so

$$T_{Wi0} = r T_{Si} + \gamma (1-r) T_{Wi-1}, \tag{10}$$

where $0 \le \gamma \le 1$. Effectively the layer sequestered below the summer mixed layer emerges with a temperature anomaly reduced by the factor γ, and by setting $\gamma = 0$ in later expressions the effect of re-emergence via persistence of anomalies in the sequestered layer can be removed.

Similarly, we introduce another process flag η in eq. (6) to monitor the contribution of preceding winter temperature anomalies that influence the following summer and winter by persisting in the summer mixed layer:

$$T_{Si0} = \eta T_{Wi-1}. \tag{11}$$

The season-to-season evolution is summarised in the schematic diagram in Fig. 1. Note that Schneider and Cornuelle (2005) introduced a similar two-season model that was integrated numerically to explore some re-emergence effects.

2.2. Season-to-season relations

The duration of each season is $\Delta t = 0.5$ yr. Equation (2) can be integrated over this time interval, using the transition relation [eq. (11)], to relate the end-of-summer state to the end-of-previous-winter state:

$$T_{Si} = f_S \eta T_{Wi-1} + (1 - f_S) Q_{Si} / \kappa_S, \tag{12}$$

where

$$f_S = \exp\{-\Delta t \kappa_S / \rho_0 c_p h_S\} \tag{13}$$

measures the fraction by which temperature anomalies are attenuated through the summer season. Similarly, from eqs. (3) and (10),

$$T_{Wi} = f_W r T_{Si} + f_W \gamma (1-r) T_{Wi-1} + (1 - f_W) Q_{Wi} / \kappa_W, \tag{14}$$

where

$$f_W = \exp\{-\Delta t \kappa_W / \rho_0 c_p h_W\}. \tag{15}$$

Thus, using eq. (12), the relation between the end-of-winter state to the end-of-previous-winter state is

$$\begin{aligned} T_{Wi} = {} & f_W [r \eta f_S + \gamma (1-r)] T_{Wi-1} \\ & + f_W r (1 - f_S) Q_{Si} / \kappa_S + (1 - f_W) Q_{Wi} / \kappa_W \end{aligned}. \tag{16}$$

The interpretation of the terms appearing in eq. (12) is as follows:

- $f_S \eta T_{Wi-1}$ is the influence of preceding winter temperature anomalies on those at the end of summer.
- $(1 - f_S) Q_{Si} / \kappa_S$ is the influence of the summer atmospheric forcing on the temperature at the end of summer.

The interpretation of the terms appearing in eq. (16) is as follows:

- $f_W r \eta f_S T_{Wi-1}$ represents the influence of preceding winter temperature anomalies that persist in the summer mixed layer, which survive after the entrainment process ends, on temperature anomalies at the end of the following winter.

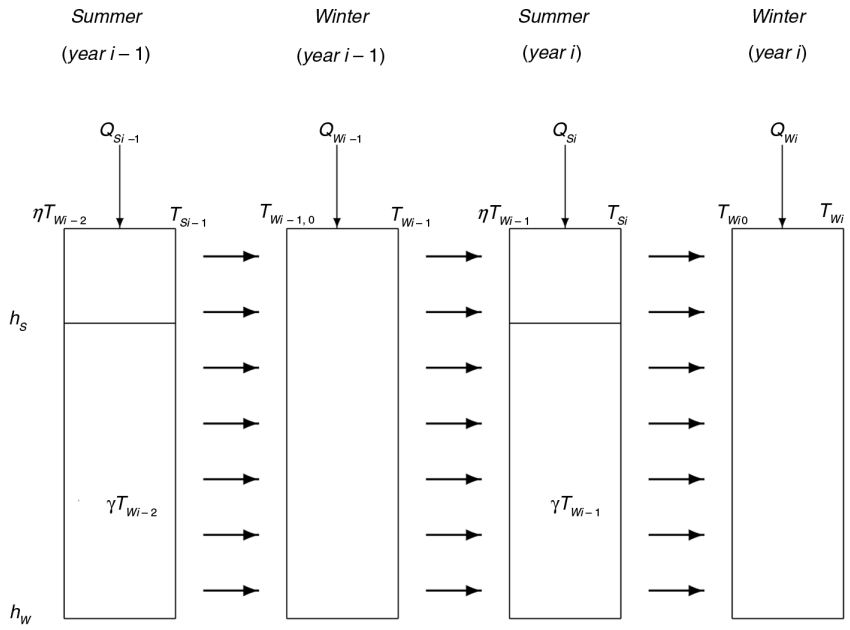

Fig. 1. Schematic of the two-season model. Note that $T_{Wi-1,0}$ represents the temperature anomaly at the start of winter in year $i-1$.

- $f_W\gamma(1-r)T_{Wi-1}$ is the influence of re-emergence on temperature anomalies at the end of the following winter.
- $f_W r(1-f_S)Q_{Si}/\kappa_S$ measures the influence of the portion of the summer atmospheric forcing that survives after the entrainment process ends on temperature anomalies at the end of the following winter.
- $(1-f_W)Q_{Wi}/\kappa_W$ measures the influence of the winter atmospheric forcing on the temperature at the end of winter.

For simplicity the model is derived in terms of end-of-season values, but note that as the thermal forcing Q is constant within each season then the end-of-season temperature is also indicative of the season-average temperature and the model could be formulated in terms of seasonal averages.

Effectively the model is an auto-regressive system. For later reference, the winter-to-winter relation, eq. (16), is written as

$$T_{Wi} = CT_{Wi-1} + R_i, \tag{17}$$

where

$$C = f_W[r\eta f_S + \gamma(1-r)], \tag{18}$$

with $0 \le C \le 1$, and

$$R_i = f_W r(1-f_S)Q_{Si}/\kappa_S + (1-f_W)Q_{Wi}/\kappa_W \tag{19}$$

is a net stochastic temperature contribution.

In particular, when $\eta = \gamma = 0$ then $C = 0$, the previous winter has no influence, and T_W evolution reduces to a white noise process.

Analytic expressions for the winter-to-winter and summer-to-winter correlations, the variance of the winter and summer temperature, and the power spectrum of the winter and summer temperature can be derived using eqs. (12) and (16), as described in the Appendix.

In exploring the effects of various parameters, departures from a set of standard values will be considered. Typical North Atlantic values of the damping parameters are $\kappa_S = 10\mathrm{Wm}^{-2}\mathrm{K}^{-1}$ and $\kappa_W = 25\mathrm{Wm}^{-2}\mathrm{K}^{-1}$ (e.g. Frankignoul et al., 1998; Deser et al., 2003). The summer mixed layer depth is fixed as $h_S = 25$ m. The selected value for the standard deviation of the winter atmospheric forcing is $\sigma_{QW} = 20\mathrm{Wm}^{-2}$, and for summer $\sigma_{QS} = 10\mathrm{Wm}^{-2}$. For reference, model variables, parameters and standard values are summarised in Table 1.

The fraction f_S decreases as the damping κ_S increases. To quantify this effect, this dependence is shown in Fig. 2a: f_S is below 0.1 when κ_S is above about $15\mathrm{Wm}^{-2}\mathrm{K}^{-1}$. Likewise, as illustrated in Fig. 2b, f_W decreases as κ_W decreases, but increases as h_W increases.

3. Analysis of the winter-to-winter correlation

As derived in the Appendix, the winter-to-winter correlation C is

$$C = \mathrm{Corr}(T_W, T_{W-1}) = f_W[r\eta f_S + \gamma(1-r)], \tag{20}$$

where

- $\eta f_W r f_S$ represents the influence of preceding winter temperature anomalies that persist in the summer mixed layer,

Table 1. Variables and parameters in the two-season model

	Description	Standard value
T_{Si}	Temperature anomaly at the end of summer i	
T_{Wi}	Temperature anomaly at the end of winter i	
Q_{Si}	Summer atmospheric forcing anomaly in year i	
Q_{Wi}	Winter atmospheric forcing anomaly in year i	
σ_{QW}	Winter forcing standard deviation	$20\mathrm{Wm}^{-2}$
σ_{QS}	Summer forcing standard deviation	$10\mathrm{Wm}^{-2}$
κ_S	Summer atmospheric damping rate	$10\mathrm{Wm}^{-2}\mathrm{K}^{-1}$
κ_W	Winter atmospheric damping rate	$25\mathrm{Wm}^{-2}\mathrm{K}^{-1}$
h_S	Summer mixed layer depth	25m
h_W	Winter mixed layer depth	250m
f_S	Summer attenuation	0.22
f_W	Winter attenuation	0.68
r	h_S/h_W	0.1
γ	Fraction of sequestered winter anomaly	1
η	Fraction of winter anomaly influencing summer layer	1
ρ_0	Ocean density	$1027\ \mathrm{Kg\ m}^{-3}$
c_p	Specific heat	$4028\ \mathrm{JKg}^{-1}\mathrm{K}^{-1}$

- $\gamma f_W(1-r)$ is the influence of re-emergence on the winter-to-winter persistence of temperature anomalies.

Note that $\mathrm{Corr}(T_W, T_{W-1})$ is the correlation found for end-of-winter values and it is independent of σ_{QW} and σ_{QS}. For end-of-winter values this property that the correlation does not depend on the stochastic forcing can also be proven for eq. (1), by considering the history of sub-mixed-layer temperatures that are created and entrained each year.

In this section, we set $\eta=\gamma=1$ and investigate the dependence of $\mathrm{Corr}(T_W, T_{W-1})$ on variations in κ_S, κ_W, and h_W, with h_S fixed to the standard value.

3.1. The impact of varying κ_S and κ_W on $Corr(T_W, T_{W-1})$

Figure 3a shows C with κ_W fixed and varying h_W and κ_S. (For reference, the black squares on this and subsequent diagrams indicate the standard values. Values of various statistics for standard values are provided in Table 2.) For large κ_S ($f_S \ll 1$) the preceding winter anomalies that influence the summer layer have negligible influence through to winter, and $C \approx f_W(1-r)$. For small κ_S ($f_S \approx 1$) the effect on C is weak. The winter depth h_W has a much larger influence on C: although C is less than 0.1 for h_W less than about 50 m, the correlation exceeds 0.5 for h_W greater than about 150 m when the re-emergence mechanism has a dominant influence.

In Fig. 3b κ_S is fixed while κ_W and h_W vary. Comparing the pattern of Fig. 3b with that of Fig. 2b, it is evident that C is strongly influenced by the attenuation factor f_W. Correlations are high for large h_W and small κ_W (e.g. larger than 0.8 when κ_W is less than about $10\ \mathrm{Wm}^{-2}\mathrm{K}^{-1}$ and h_W larger than 250 m), when a relatively large heat content is sequestered for re-emergence.

It is interesting to compare the winter-to-winter correlation with the value when $r=1$. Let C_1 denote the winter-to-winter correlation when $r=1$. From (20),

$$C_1 = \eta f_{W1} f_S, \tag{21}$$

where f_{W1} is the value of f_W when $r=1$. Then

$$C - C_1 = \eta f_S(r f_W - f_{W1}) + \gamma f_W(1-r), \tag{22}$$

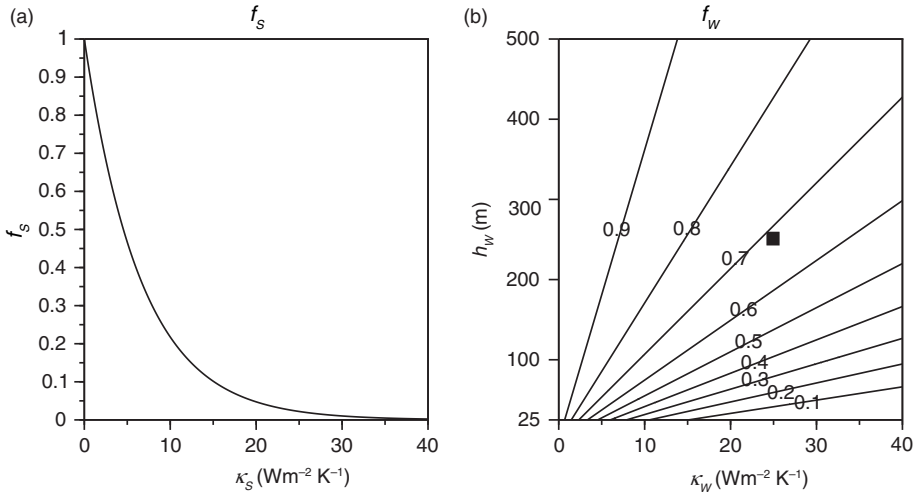

Fig. 2. (a) Dependence of the summer attenuation factor f_S on the damping rate κ_S, with $h_S=25$ m; (b) dependence of the winter attenuation factor f_W on damping rate κ_W and depth h_W.

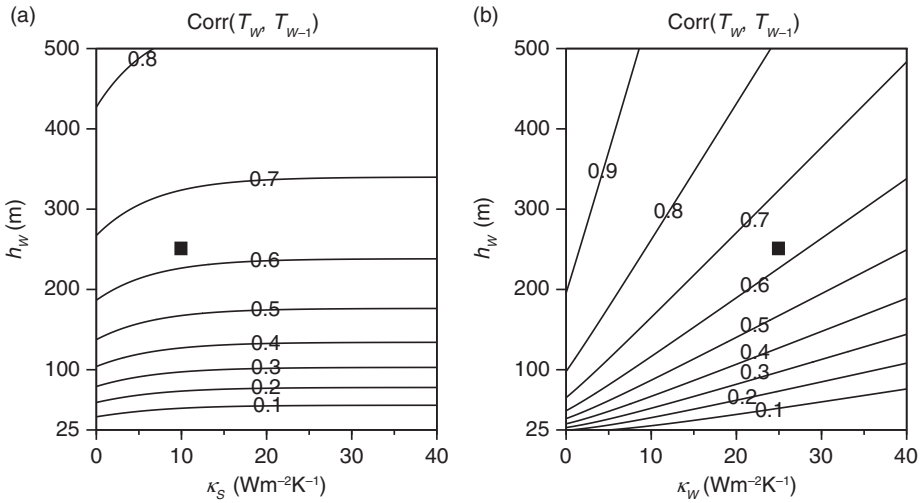

Fig. 3. Winter-to-winter correlation Corr(T_W, T_{W-1}): (a) dependence on summer damping rate κ_S and winter depth h_W, (b) dependence on winter damping rate κ_W and depth h_W.

where $\eta f_S(rf_W - f_{W1})$ represents the contribution of persistence via the summer mixed layer. When $\eta = \gamma = 1$ it is straightforward to prove that $C > C_1$ when $h_W > h_S$. Since $f_{W1} < f_W$ for all $h_W > h_S$, and $f_S < 1$,

$$\begin{aligned} C_1 &= f_{W1}f_S < f_W f_S = rf_W f_S + (1-r)f_W f_S \\ &< f_W[rf_S + 1 - r] = C, \end{aligned} \tag{23}$$

which concludes the proof. The term rf_W appears often in the properties of the model, and for reference it is illustrated in Fig. 4 for a range of values of h_W and κ_W. As a function of h_W this term has a maximum at a depth $h_W = \Delta t \kappa_W / \rho_0 c_p$. When κ_W is less than about 7 Wm^{-2}K^{-1} that depth is less than h_S, and in Fig. 4 rf_W decreases as h_W increases. For larger κ_W, rf_W increases to a maximum and then decreases as h_W increases. The line with $rf_W = f_{W1}$ is also included in Fig. 4. Below this line persistence increases $C - C_1$, but above the line persistence decreases $C - C_1$.

This behaviour occurs due to the competing effects of h_W: increasing the winter mixed layer depth reduces the relative contribution of preceding winter temperature anomalies via persistence, but also reduces the rate at which they are damped through winter.

The relative effects of re-emergence and persistence on the winter-to-winter correlation as h_W varies can be compared. From eq. (20), with $\eta = \gamma = 1$, the former is larger than the latter when $(1-r) > rf_S$. This condition (which is independent of κ_W) can be re-written as $h_W > (1+f_S)h_S$, and as $0 < f_S < 1$, it follows that re-emergence always has the larger influence when $h_W > 2h_S$.

To quantify the relative effects, the ratio $rf_S/(1-r)$ is shown in Fig. 5 for varying h_W and κ_S. The ratio rapidly decreases as h_W increases, the more so as κ_S increases. For the standard value $\kappa_S = 10$Wm^{-2}K^{-1} the ratio is 1 for $h_W \approx 30$ m, but less than 0.2 when $h_W > 52$ m. Unless the seasonal range of mixed layer depth is small, re-emergence has a much larger influence on the winter-to-winter persistence of temperature anomalies than that of preceding winter temperature anomalies that persist through the summer mixed layer.

Table 2. Statistics for standard values in the two-season model

Corr(T_W, T_{W-1})	0.63
Corr(T_W, T_S)	0.21
σ_R	0.26 W^{2}m^{-4}
σ_{TW}	0.33 K^2
σ_{TS}	0.79 K^2
α	2.4
P_W (0)	0.49 K^2
P_W (0.5)	0.03 K^2
G_W (0)	7.3
G_W (0.5)	0.38

4. Analysis of the winter temperature variance

As derived in the Appendix, the winter temperature variance σ^2_{TW} is

$$\sigma^2_{TW} = \sigma^2_R/(1 - C^2), \tag{24}$$

where

$$\sigma^2_R = \sigma^2_{RS} + \sigma^2_{RW} \tag{25}$$

is determined by the random stochastic forcing, with

$$\begin{aligned} \sigma^2_{RS} &= r^2 f^2_W (1-f_S)^2 (\sigma^2_{QS}/\kappa^2_S), \\ \sigma^2_{RW} &= (1-f_W)^2 (\sigma^2_{QW}/\kappa^2_W). \end{aligned} \tag{26}$$

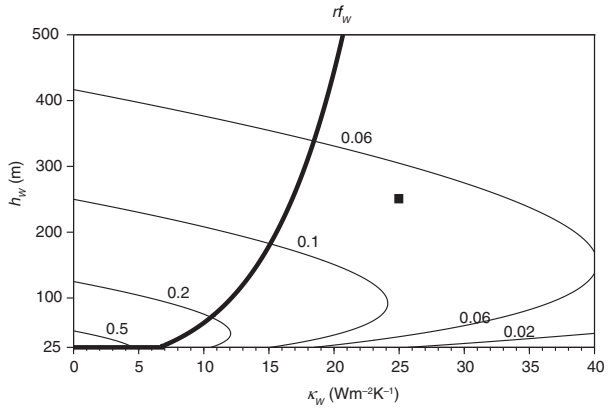

Fig. 4. Dependence of rf_W on the damping rate κ_W and depth h_W. The thick line indicates where, for each κ_W, $rf_W = f_{W1}$.

Overall the magnitude of σ^2_{TW} is determined by σ^2_R, modified by the effect of C. (Note that σ_R does not depend on the process parameters η and γ.) When $\eta = \gamma = 0$ then $C = 0$, T_W is a white noise process, and $\sigma_{TW} = \sigma_R$. When preceding winter has an influence, then $C > 0$ and σ_{TW} is amplified above σ_R.

Both C and σ_R depend on several model parameters, and in this section the effect of parameter variations on σ_{TW} and its components is explored and quantified. For this purpose it is convenient to rewrite eq. (24) as

$$\sigma^2_{TW} = \sigma^2_R + \sigma^2_P, \tag{27}$$

where

$$\sigma^2_P = \sigma^2_R C^2/(1 - C^2) \tag{28}$$

contains the influence of preceding winters in the process. The fraction of variance associated with preceding winters is $\sigma^2_P/\sigma^2_{TW} = C^2$, and is the fraction that would be predictable from preceding winter information using a linear regression approach based on eq. (17). Furthermore, the fraction of the variance due to random forcing alone is $\sigma^2_R/\sigma^2_{TW} = 1 - C^2$, which is independent of the summer and winter atmospheric variability. When $C^2 > 0.5$, σ^2_P makes a larger contribution to σ^2_{TW} than the random component σ^2_R.

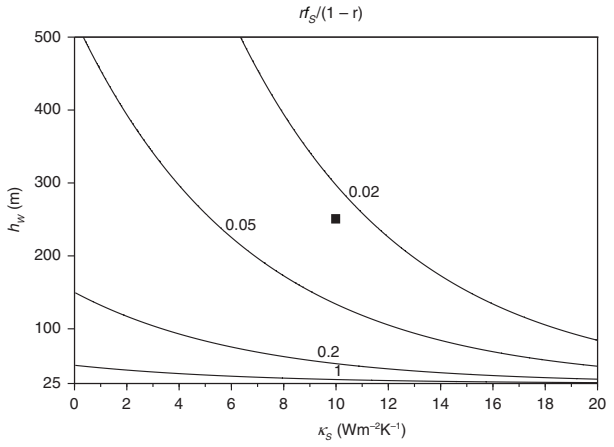

Fig. 5. Dependence of $rf_S/(1-r)$ on summer damping rate κ_S and winter depth h_W.

4.1. *The impact of varying κ_W and h_W on σ^2_{TW}*

Figure 6 illustrates the effect of varying h_W and κ_W on the winter variance, with other parameters set to standard values. As shown in Fig. 6a, σ^2_{TW} is largest when $h_W = h_S$ and $\kappa_W = 0$. (Note that as $\kappa_W \to 0$ then $(1 - f_W)/\kappa_W \to \Delta t/\rho_0 c_p h_W$ and thus remains finite.) As expected, σ^2_{TW} decreases as damping κ_W increases. For fixed κ_W, σ^2_{TW} decreases as h_W increases, because the increased heat capacity of the deeper winter layer means less temperature change for the same heat input.

The region with $C = 0.7$ in Fig. 3b indicates approximately when the contribution to σ^2_{TW} from σ^2_P is greater than that of σ^2_R (i.e. when $C^2 > 0.5$). For $\kappa_W \to 0$ this occurs when h_W is greater than about 70 m, and occurs at larger h_W as κ_W increases. For all κ_W, when h_W is very close to h_S, $\sigma^2_{TW} \approx \sigma^2_R$ and when h_W is close to 500 m, $\sigma^2_{TW} \approx \sigma^2_P$.

The winter and summer components σ^2_{RS} and σ^2_{RW} are plotted similarly in Fig. 7. (The 'summer' component depends on κ_W because the anomalies imposed in the summer season are attenuated through the following winter.) For the ranges of values shown σ^2_{RW} (Fig. 7a) decreases as κ_W and h_W increase, and is much larger than σ^2_{RS} (Fig. 7b). σ^2_{RS} is negligible for all h_W because when h_W is close to h_S anomalies forced in the preceding summer are relatively strongly damped in a shallow winter mixed layer, whereas for larger h_W entrainment acts to significantly reduce their influence. Note that for κ_W above about 6 Wm^{-2}K^{-1}, σ^2_{RS} increases at first as h_W increases from h_S, then decreases: this is due to the effect of the factor rf_W as described in Section 3.1.

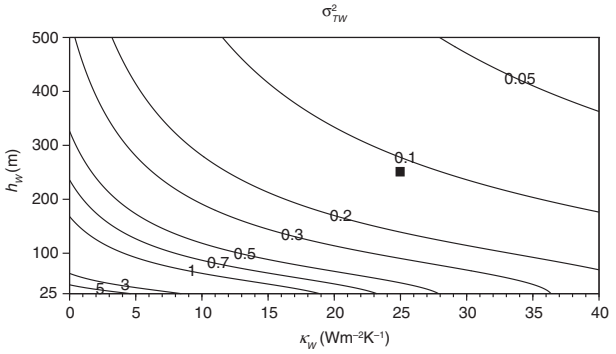

Fig. 6. Dependence of the winter variance σ^2_{TW} on damping rate κ_W and depth h_W.

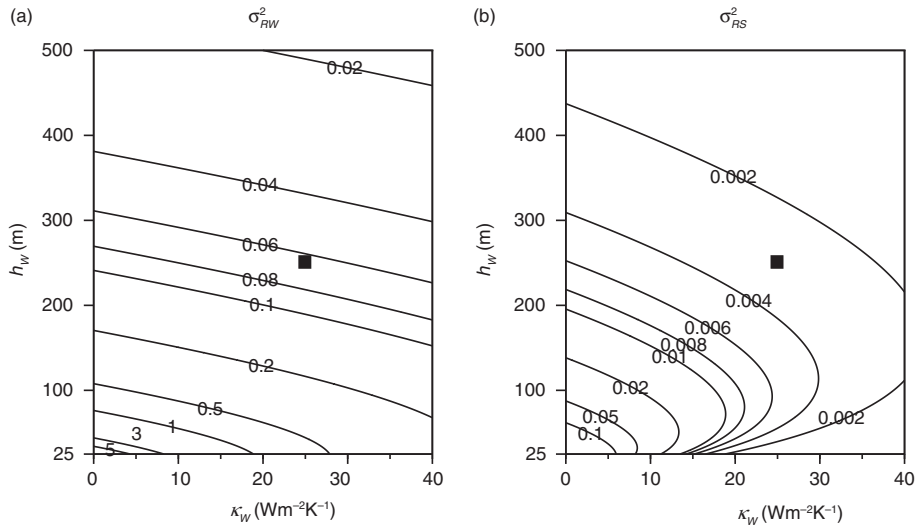

Fig. 7. Winter variance components associated with the random forcing. (a) dependence of σ^2_{RW} on winter damping rate κ_W and depth h_W, (b) likewise for σ^2_{RS}.

The relative effects on σ_{TW} of the near-surface and sequestered pathways for winter-to-winter connections are explored by plotting σ^2_P for $\gamma = 1$, $\eta = 0$ (Fig. 8a, sequestered path only) and for $\gamma = 0$, $\eta = 1$ (Fig. 8b, near-surface path only). Except for depths h_W close to h_S, the sequestered path has a much greater effect. Note that the behaviour of σ^2_P with h_W when $\gamma = 0$ and $\eta = 1$ (Fig. 8b) is similar to that which was described for σ^2_{RS}, with the effect of the term rf_W again evident. It is also interesting to note that when $\gamma = 1$, $\eta = 0$, σ^2_P increases as h_W increases from h_S, and then decreases. This is linked to the effects of decreasing the winter mixed layer depth on the effects of the atmospheric forcing and re-emergence: decreasing (increasing) the winter mixed layer increases (decreases) the size of the temperature anomalies via the atmospheric forcing, which acts to increase (decrease) the effects of re-emergence on the temperature in the following winter.

4.2. *The impact of varying κ_S and σ_{QW}* on σ^2_{TW}

As shown in Fig. 9a, σ^2_{TW} varies little as the summer damping coefficient κ_S varies. The apparent greater sensitivity for larger h_W is due to the substantially reduced values of σ^2_{TW} for larger h_W.

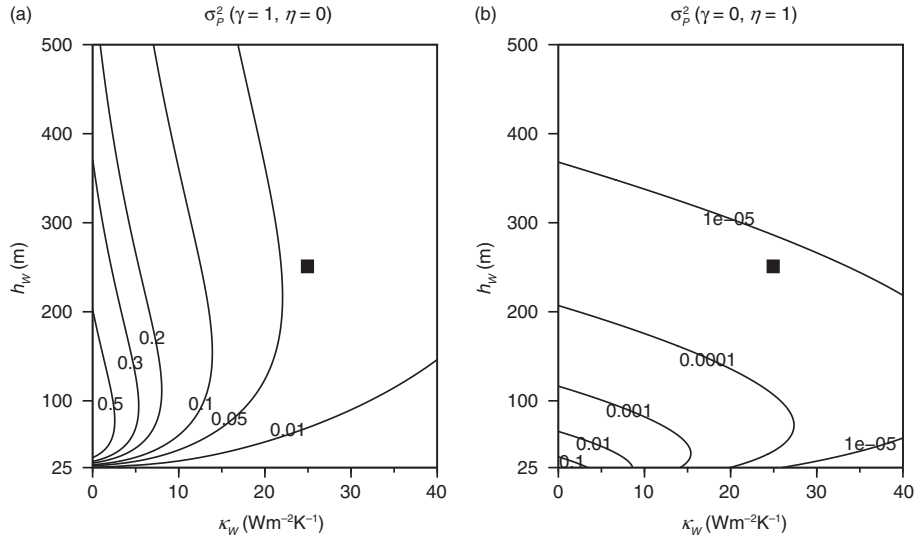

Fig. 8. Dependence of the predictable component of winter variance σ^2_P on winter damping rate κ_W and depth h_W: (a) process flags $\gamma = 1$, $\eta = 0$, (b) $\gamma = 0$, $\eta = 1$.

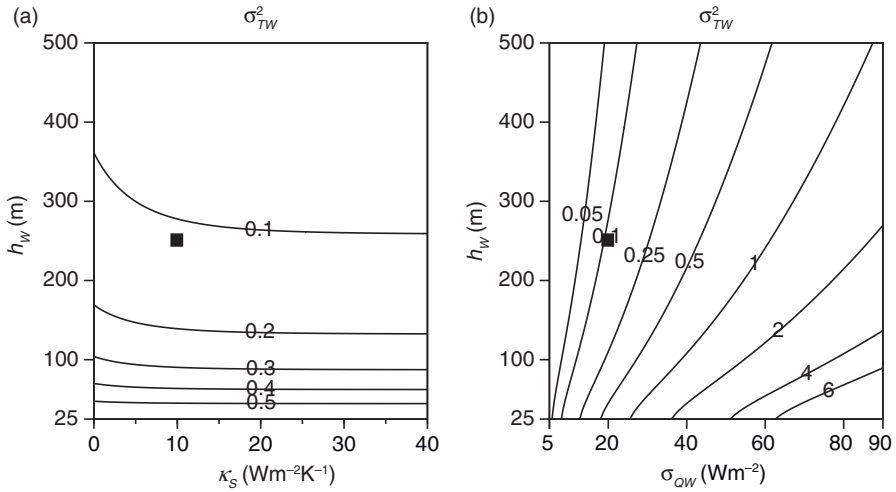

Fig. 9. Winter variance σ^2_{TW} (a) dependence on summer damping κ_S and winter depth h_W, (b) dependence on winter random forcing σ^2_{QW} and depth h_W.

Figure 9b quantifies the response of σ^2_{TW} to σ_{QW}. As expected, increasing the winter forcing σ_{QW} increases σ^2_{TW} (roughly quadratically), by increasing present winter and previous winter temperature variances, with less sensitivity for larger h_W.

5. The power spectrum of the winter temperature

From the winter-to-winter relation in eq. (17), the power spectrum of the winter temperature, $P_W(\omega)$, can be derived. Equation (A25) gives

$$P_W(\omega) = \sigma^2_R \; G_W(\omega), \tag{29}$$

where

$$G_W(\omega) = 1/[1 - 2C\cos(2\pi\omega) + C^2] \tag{30}$$

is the shape function that depends only on the winter-to-winter correlation C, and frequency $\omega \in [0, 0.5]$ corresponds to periods from 2 yr upwards. Preceding winter conditions act to decrease power for short (interannual) periods, and increase power at long periods, with the crossover at $G_W = 1$ when $\cos(2\pi\omega) = C/2$. For standard values, the crossover occurs at a period of 5 yr.

5.1. The effect of re-emergence and preceding winter temperature anomalies that persist in the summer mixed layer on P_W

The expression for the power spectrum of the winter temperature enables us to establish the influence of re-emergence, of preceding winter temperature anomalies that persist in the summer mixed layer, and of summer atmospheric forcing, for a range of timescales. Various winter spectra are illustrated in Fig. 10, using standard values.

When $\gamma = \eta = 0$, $G_W(\omega) = 1$ for all ω, and eq. (29) reduces to $P_W(\omega) = \sigma^2_R$. When there are no effects of re-emergence and preceding winter temperatures that persist in summer the power spectrum is flat, as shown by the thin black line in Fig. 10.

When $\eta = 0$ and $\gamma = 1$, $C = f_W(1 - r)$ in eq. (30) and only the effects of re-emergence influence P_W. This case is shown by the thick line in Fig. 10. The shape factor has $G_W(0) = 6.7$, $G_W(0.5) = 0.4$.

For $\gamma = 0$ and $\eta = 1$, $C = rf_W f_s$, and P_W is only influenced by preceding winter temperature anomalies that persist in the summer mixed layer. This case is illustrated by the broken line in Fig. 10: the effect of persistence on P_W is much weaker than that of re-emergence, as evident in the shape factor values $G_W(0) = 1.03$, $G_W(0.5) = 0.97$.

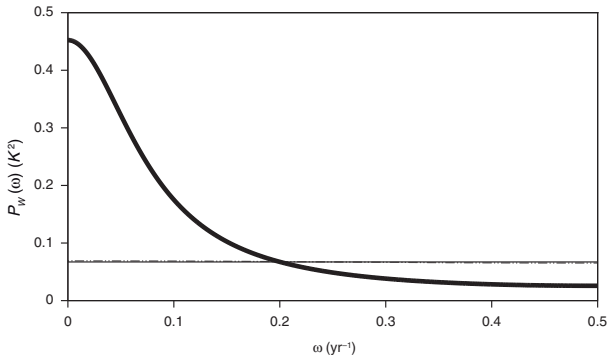

Fig. 10. Power spectrum $P_W(\omega)$ of winter temperature anomalies for standard parameter values and various combinations of process flags. Solid line $\gamma = 0$, $\eta = 0$; dashed line $\gamma = 0$, $\eta = 1$; thick line $\gamma = 1$, $\eta = 0$. Note that the thin solid and dashed lines nearly coincide.

With persistence and re-emergence processes included ($\eta = \gamma = 1$), for standard values the spectrum is very similar to that with re-emergence only. The graph for this case is included in the parameter comparisons shown in Fig. 11. Note that re-emergence reddens the winter temperature spectrum.

Schneider and Cornuelle (2005) described spectra from numerical integrations with a similar two-season model, in which re-emergence increased the spectral power at interannual timescales but not at longer timescales. One reason for the contrast with our result is the experimental design. They compare spectra from an integration with a constant deep (winter) mixed layer with that from an integration with deep winter and shallow summer layers, whereas in our experiments there is always a deep winter and shallow summer layer and spectral comparisons are made by varying the 'process flags' and parameters. In their comparison, decreasing the summer mixed layer depth increases the variability of the mixed layer temperature in summer, which results in an increase in the spectral power of the mixed layer temperature at interannual and shorter timescales. A further difference is the throughout-season data sampling in Schneider and Cornuelle (2005) versus the end-of-season sampling in our results. An increase in spectral power at decadal timescales was also found in the study with idealised models by De Coëtlogon and Frankignoul (2003), in which they compared spectra from an integration with a constant e-folding scale of 3 months and an integration with the addition of a simple re-emergence term in winter.

5.2. *The effect of varying κ_S, κ_W and h_W on P_W*

In this section, the effect of varying κ_S, κ_W and h_W on P_W is investigated. Throughout this section, we set $\gamma = \eta = 1$, and the reference case (represented by the thin lines in Fig. 11) uses standard values.

The thick line in Fig. 11a shows P_W when the winter atmospheric damping κ_W is increased to $40\mathrm{Wm}^{-2}\mathrm{K}^{-1}$. Increasing κ_W reduces σ_R^2, and also decreases C with the effect of flattening the shape of the spectrum. At interannual timescales these effects offset each other, and in this example the net result is very small [P_W (0.5) reduces from 0.025 to 0.024], whereas at decadal timescales the effects reinforce and the power is more than halved for P_W (0).

The thick line in Fig. 11b shows P_W when the summer atmospheric damping is increased to $40\mathrm{Wm}^{-2}\mathrm{K}^{-1}$. The system is less sensitive to κ_S, and in this case the power is reduced slightly.

The thick line in Fig. 11c shows P_W when the winter mixed layer depth is doubled to 500m. The term σ_R^2 is more than halved, but C is increased so the shape factor is steepened. The effects offset at long timescales, and the result in this case is a slight reduction of $P_W(0)$ from 0.49 to 0.48. The effects re-inforce at interannual scales, and $P_W(0.5)$ is reduced by about 75%.

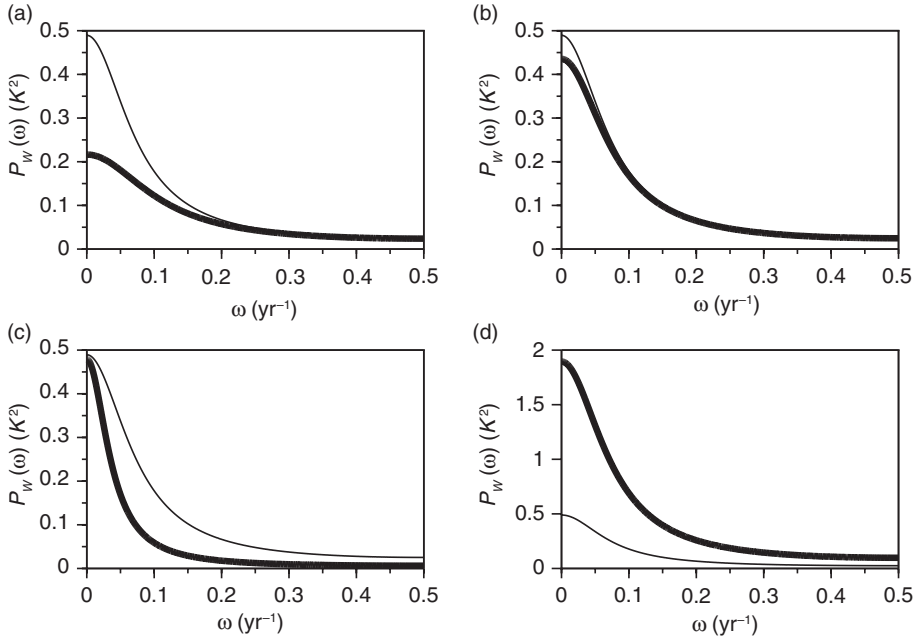

Fig. 11. Power spectrum $P_W(\omega)$ of winter temperature anomalies. In each case the thin line is $P_W(\omega)$ for standard values, the thick line for parameter variations. (a) winter damping κ_W increased to 40 $\mathrm{Wm}^{-2}\mathrm{K}^{-1}$, (b) summer damping κ_S increased to 40 $\mathrm{Wm}^{-2}\mathrm{K}^{-1}$, (c) winter depth h_W doubled to 500 m, (d) winter random forcing σ_{QW} doubled to 40 Wm^{-2}.

Figure 11d shows how doubling σ_{QW} (thick line) acts to increase the winter temperature variability at all timescales, by increasing σ_R^2 without affecting $G_W(\omega)$.

6. Analysis of variances and the summer-to-winter correlation

A measure of the influence of re-emergence is the relative values of winter-to-winter correlation and summer-to-winter correlation. This involves in part the relative variances of summer and winter temperature anomalies, which are themselves of interest. Analytic expressions for these quantities are presented and analysed in this section.

The ratio of the summer and winter standard deviations of the temperature σ_{TS}/σ_{TW} is denoted α. Expressions for the variances σ_{TS}^2 and σ_{TW}^2 are derived in the Appendix. Note that these are related by

$$\sigma_{TS}^2 = f_S^2\eta^2\sigma_{TW}^2 + (1-f_S)^2\sigma_{QS}^2/\kappa_S^2. \tag{31}$$

The expressions in the Appendix lead to

$$\alpha^2 = f_S^2\eta^2 + \frac{(1-C^2)}{r^2 f_W^2 + (\sigma_{QW}^2/\sigma_{QS}^2)(\kappa_S^2/\kappa_W^2)(1-f_W)^2/(1-f_S)^2}. \tag{32}$$

Note that when the 'process flags' η and γ are zero (so winter and summer are disconnected from the conditions in the previous winter, and $C=0$) the expression reduces to

$$\alpha^2 = \frac{1}{r^2 f_W^2 + (\sigma_{QW}^2/\sigma_{QS}^2)(\kappa_S^2/\kappa_W^2)(1-f_W)^2/(1-f_S)^2}. \tag{33}$$

When re-emergence is activated by setting $\gamma=1$ then C increases and α decreases, so re-emergence decreases the ratio of σ_{TS} to σ_{TW}.

The covariance of summer and following winter anomalies (see Appendix A.2.3) can be written

$$\mathrm{Cov}(T_W, T_S) = f_W f_S r\eta^2\sigma_{TW}^2 + f_W f_S\eta\gamma(1-r)\sigma_{TW}^2 + f_W(1-f_S)^2 r\sigma_{QS}^2/\kappa_S^2. \tag{34}$$

The first term is due to the previous winter influencing the summer which in turn influences the following winter; the second term is due to the previous winter influencing the following winter through re-emergence; and the third term is due to the summer forcing of summer anomalies that influence the following winter. The first and third terms can be combined to obtain

$$\mathrm{Cov}(T_W, T_S) = f_W r\sigma_{TS}^2 + f_W f_S\eta\gamma(1-r)\sigma_{TW}^2, \tag{35}$$

from which it follows that the summer-to-following-winter correlation is

$$\mathrm{Corr}(T_W, T_S) = f_W r\alpha + f_W f_S\eta\gamma(1-r)/\alpha. \tag{36}$$

The terms in eq. (36) are interpreted as follows:

- $f_W r\alpha$ represents the influence of summer temperature anomalies (due to both summer forcing and previous winter persistence) on those in the following winter.
- $f_W f_S\eta\gamma(1-r)/\alpha$ is a contribution due to the influence of preceding winter temperature anomalies on T_W through re-emergence. Note that the process flag η also appears here: when $\eta=0$ re-emergence still occurs, but the re-emerging anomalies have no correlation with T_S as T_S is determined only by Q_S when $\eta=0$.

Thus Corr(T_W, T_S) is not just a measure of the impact of summer temperature anomalies on those in the following winter.

6.1. *The impact of varying κ_W and h_W on Corr(T_W, T_S) and α*

The effect of varying κ_W and h_W, with other parameters set to standard values and $\eta=\gamma=1$, is described here. The effect on the summer-to-following-winter correlation Corr(T_W, T_S) is illustrated in Fig. 12a. As expected, for fixed h_W the correlation decreases as the winter damping κ_W increases. The correlation is small for h_W close to h_S except when winter damping is small: when winter depths are small the anomalies induced by the random winter forcing dominate the influence of previous seasons. The correlation then increases as h_W increases, then decreases: it is largest (over 0.4) for small κ_W and for h_W about 75 m. For the standard value $\kappa_W = 25\,\mathrm{Wm^{-2}K^{-1}}$ correlation exceeds 0.2 for h_W ranging from 100 to 400 m. Comparing the pattern in Fig. 3b with that of Fig. 12a, it is clear that Corr(T_W, T_S) is not as strongly influenced by variations in h_W as Corr(T_W, T_{W-1}).

As shown in Fig. 12b, the ratio σ_{TS}/σ_{TW} increases as κ_W increases. As σ_{TW} decreases as winter damping increases, it is evident from eq. (31) that σ_{TS} also decreases but α increases as κ_W increases. Likewise the ratio also increases as h_W increases, because σ_{TW} decreases. For the parameter values used, the ratio is larger than 1 when h_W is larger than about 200 m when κ_W is small.

The contributions to the correlation from the two terms in eq. (35) are provided in Fig. 12c and d. In Fig. 12c the pattern is again linked to that of rf_W described in Section 3.1. For the 're-emergence' term in Fig. 12d, this contribution is largest for small κ_W, with a maximum at around $h_W = 100$ m for small κ_W. (The maximum is a result of the trade-off between increasing $(1-r)f_W$ and decreasing $1/\alpha$ as h_W increases. As h_W increases, the amount of re-emerging water increases but the variance of its temperature decreases. This feature

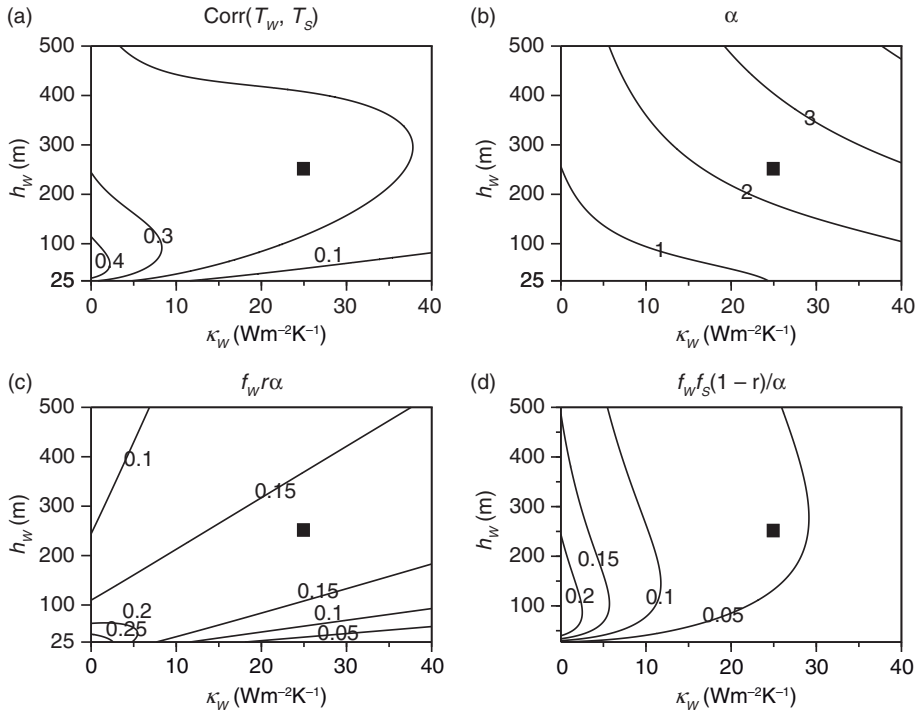

Fig. 12. Dependence of summer and winter relations on the winter damping rate κ_W and depth h_W (a) the summer-to-winter correlation Corr(T_W, T_S), (b) the ratio $\alpha = \sigma_{TS}/\sigma_{TW}$, (c) the component $f_W r\alpha$ of Corr(T_W, T_S), (d) the component $f_W f_S(1-r)/\alpha$ of Corr(T_W, T_S).

influences the occurrence and location of the maximum in correlation in Fig. 12a.) The two terms are similar in size: persistence of anomalies in surface layers and re-emergence of sub-surface information are both influential in the overall correlation between summer and following winter temperature anomalies. For the standard winter damping value $\kappa_W = 25\text{Wm}^{-2}\text{K}^{-1}$ re-emergence is less influential than the other term.

6.2. The impact of varying κ_S and h_W on Corr(T_W, T_S) and α

Similarly the effect of varying κ_S and h_W is illustrated in Fig. 13. In Fig. 13a it can be seen that Corr(T_W, T_S) decreases as κ_S increases and summer anomalies are reduced. For h_W close to h_S the correlation is small (as in Fig. 12a). As h_W increases from h_S the correlation increases, and then weakly decreases for h_W larger than about 200 m. For low κ_S the correlation exceeds 0.4 for h_W between about 125 and 375 m. Comparing Fig. 3a with Fig. 13a, it is clear that Corr(T_W, T_S) is more sensitive to variations in κ_S than Corr(T_W, T_{W-1}).

The ratio α, shown in Fig. 13b, decreases as κ_S increases: while increasing the summer damping reduces both summer and winter variances, the more direct effect on the summer variance is greater. Similar to Fig. 12b, for fixed κ_S the ratio increases as h_W increases and winter variances decrease. Small κ_S favours larger summer variance, and α is largest for low κ_S and large h_W.

The components of the correlation are provided in Fig. 13c and d. For small fixed κ_S the term $f_W r\alpha$ in Fig. 13c has a maximum at h_W about 200 m. This contrast to the pattern in Fig. 12c occurs because α now increases as h_W increases. Both terms have similar behaviour as κ_S and h_W vary, with $f_W r\alpha$ generally more than twice the re-emergence contribution.

6.3. The impact of varying σ_{QW} on Corr(T_W, T_S) and α

Changing the winter forcing standard deviation σ_{QW} changes the winter temperature variance correspondingly. The effect on Corr(T_W, T_S) and α is explored here by varying σ_{QW} and h_W with other parameters set to their default values. (Note that the default for σ_{QS} is 10Wm^{-2}, the default for σ_{QW} is $20\,\text{Wm}^{-2}$, and σ_{QW} ranges from 5 to $90\,\text{Wm}^{-2}$ in the results illustrated.)

Figure 14a shows Corr(T_W, T_S). For small σ_{QW} the random forcing of winter anomalies is weak and anomalies from the previous summer can have a stronger influence:

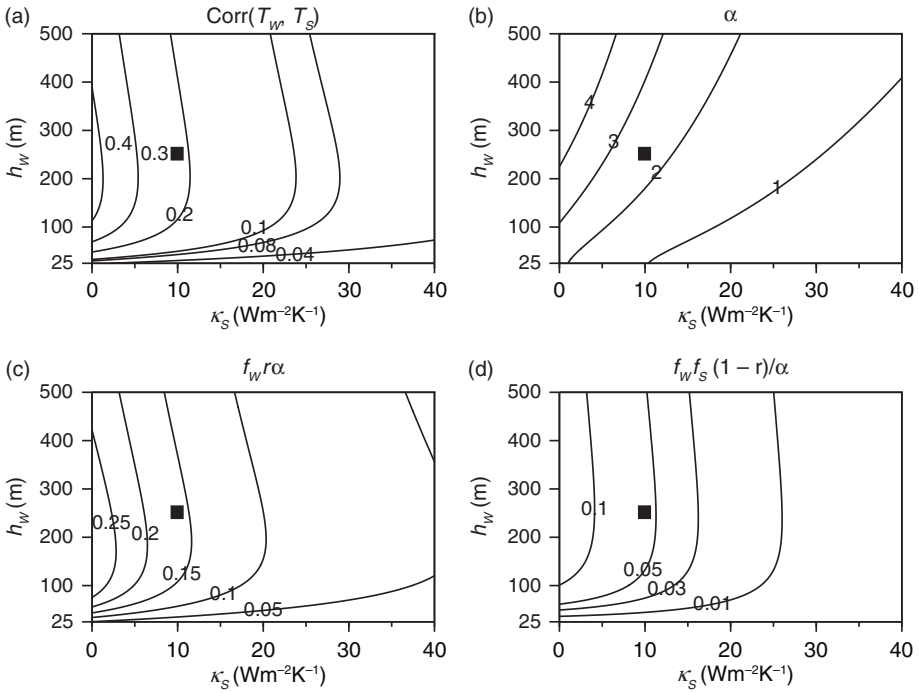

Fig. 13. Dependence of summer and winter relations on the summer damping rate κ_S and winter depth h_W (a) the summer-to-winter correlation Corr(T_W, T_S), (b) the ratio $\alpha = \sigma_{TS}/\sigma_{TW}$, (c) the component $f_W r\alpha$ of Corr(T_W, T_S), (d) the component $f_W f_S(1-r)/\alpha$ of Corr(T_W, T_S).

thus the largest values in Fig. 14a occur with σ_{QW} at the low end of the range, reaching about 0.5 when h_W is in the range 100–250 m. As σ_{QW} increases from 5 Wm^{-2} the correlations decrease at first, but then increase again for σ_{QW} larger than 40 Wm^{-2}. The reason is that the re-emergence contribution to the correlation increases as σ_{QW} increases and winter variance increases. This is clear from the two contributions to the correlation mapped in Fig. 14c and d: for small σ_{QW} $f_W r\alpha$ in Fig. 14c dominates, while for large σ_{QW} $f_W f_S(1-r)/\alpha$ dominates.

This behaviour is related to the effect of σ_{QW} on α shown in Fig. 14b. Decreasing σ_{QW} decreases both σ_{TW} and σ_{TS}, but the effect is relatively larger for σ_{TW}. Consequently the ratio α increases markedly as σ_{QW} decreases below about 20 Wm^{-2}, particularly for larger h_W. Increasing σ_{QW} above the default value of 20 Wm^{-2} has a weak decreasing effect on α.

For h_W close to h_S the correlation is weak for all σ_{QW} in the example.

7. Measures of the re-emergence signal

In previous studies, such as Timlin et al. (2002) and Deser et al. (2003), which show that the effect of summer SSTs on those in the following winter is weaker than that of preceding winter temperature anomalies, the winter-to-preceding winter value of the SST ACF is substantially larger than the winter-to-preceding summer value. The re-emergence signal can therefore be characterised by the ratio

$$R = \mathrm{Corr}(T_W, T_{W-1})/\mathrm{Corr}(T_W, T_S),$$

which can be expressed analytically using eqs. (20) and (36):

$$R = [\eta r f_S + \gamma(1-r)]/[r\alpha + \gamma\eta(1-r)f_S\alpha^{-1}]. \quad (37)$$

Thus, summer temperature anomalies are having a relatively weak impact on the winter-to-winter persistence of temperature anomalies if $R \gg 1$ and vice versa if R is small.

As was shown in the previous section, Corr(T_W, T_S) includes a re-emergence component and overestimates the direct impact of summer temperature anomalies on those in the following winter. An alternative that can be assessed in the two-season formulation (but is more difficult to calculate from observations) is to use the correlation between winter temperature and the summer temperatures produced by the random atmospheric forcing, which is the same as the correlation Corr(T_W, Q_S), as a measure of the direct summer-to-winter relation. The alternative ratio is

$$R^* = \mathrm{Corr}(T_W, T_{W-1})/\mathrm{Corr}(T_W, Q_S). \quad (38)$$

From eq. (16)

$$\mathrm{Cov}(T_W, Q_S) = f_W r(1-f_S)\sigma_{QS}^2/\kappa_S. \quad (39)$$

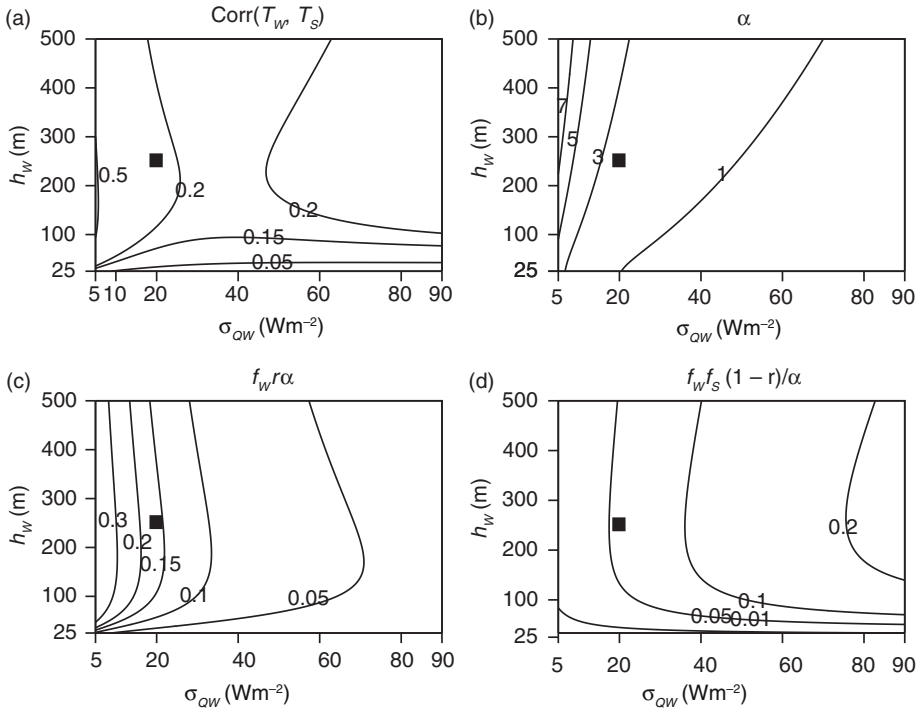

Fig. 14. Dependence of summer and winter relations on the winter forcing σ_{QW} and depth h_W (a) the summer-to-winter correlation Corr(T_W, T_S), (b) the ratio $\alpha = \sigma_{TS}/\sigma_{TW}$, (c) the component $f_W r\alpha$ of Corr(T_W, T_S), (d) the component $f_W f_S(1-\mathrm{r})/\alpha$ of Corr(T_W, T_S).

Making use of the expression for σ_{TW}^2 in eq. (A6), the analytic expression for Corr(T_W, Q_S) is

$$\mathrm{Corr}(T_W, Q_S) = f_W r\alpha^*, \tag{40}$$

where [cf. eq. (32)]

$$\alpha^{*2} = \frac{(1-C^2)}{r^2 f_W^2 + (\sigma_{QW}^2/\sigma_{QS}^2)(\kappa_S^2/\kappa_W^2)(1-f_W)^2/(1-f_S)^2}. \tag{41}$$

Thus

$$R^* = [\eta r f_S + \gamma(1-r)]/r\alpha^*. \tag{42}$$

For standard values, when $r = 1$ and re-emergence has no role R and R^* have similar values of about 0.2. R and R^* both increase as h_W increases, with R^* larger than R: for standard values, when $h_W = 500$ m R is about 4, R^* about 6.

7.1. The response of R and R^* to varying κ_W, κ_S and σ_{QW}

Unless otherwise stated, parameters have their default values and $\eta = \gamma = 1$. Figure 15a and b show R and R^* when κ_W and h_W are varied and other parameters have their default values. R and R^* have similar relatively low values for h_W close to h_S, and increase as h_W increases. R is not very sensitive to κ_W, whereas R^* increases more rapidly with depth when κ_W is small. For small winter damping κ_W winter temperature variance is relatively large and re-emergence has a stronger effect, and this influence is emphasised in R^*.

As seen in Fig. 15c and d the effect of varying summer damping κ_S is very similar for R and R^*. In this example the largest values are found for large h_W and large κ_S, because summer temperature anomalies are strongly damped by large κ_S and re-emergence again has a stronger effect.

The effect of varying winter forcing σ_{QW} is illustrated in Fig. 15e and f. Differences between R and R^* are most evident for larger σ_{QW}. For σ_{QW} larger than 40Wm^{-2}, R decreases but R^* increases markedly as σ_{QW} increases. This occurs because winter temperature variance increases as σ_{QW} increases: the re-emergence component maintains Corr(T_W, T_S) in R (cf. Fig. 14a), while Corr(T_W, Q_S) decreases in R^*.

8. Statistics for the summer temperature

8.1. The summer-to-summer correlation

As derived in the Appendix, the summer-to-summer correlation is

$$\mathrm{Corr}(T_S, T_{S-1}) = \eta f_S \mathrm{Corr}(T_W, T_S)/\alpha. \tag{43}$$

When $\eta = 0$, Corr(T_S, T_{S-1}) = 0, that is, preceding summer temperatures cannot influence the summer temperature if

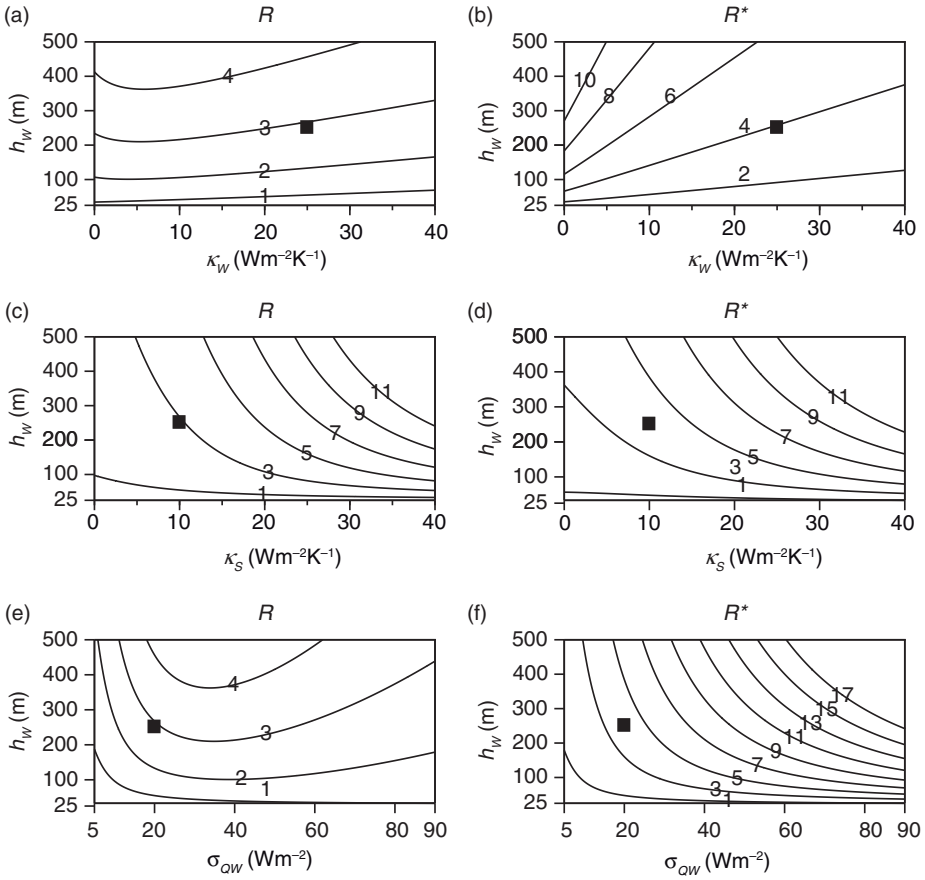

Fig. 15. Parameter dependence of the correlation ratios $R = \mathrm{Corr}(T_W, T_{W-1})/\mathrm{Corr}(T_W, T_S)$ and $R^* = \mathrm{Corr}(T_W, T_{W-1})/\mathrm{Corr}(T_W, Q_S)$. (a) R and (b) R^* dependence on κ_W and h_W; (c) R and (d) R^* dependence on κ_S and h_W; (e) R and (f) R^* dependence on σ_{QW} and h_W.

winter temperatures do not influence the summer temperature. (a), (b) and (c) of Fig. 16 show how $\mathrm{Corr}(T_S, T_{S-1})$ varies with h_W, κ_W, κ_S and σ_{QW} with other parameters in each figure set to their default values. It is clear that, as expected, preceding summer temperatures have little influence on those in the following summer for the ranges of parameters considered here.

8.2. The power spectrum of the summer temperature

As derived in the Appendix, the power spectrum of the summer temperature is

$$P_S(\omega) = \sigma_{TS}^2 G_S(\omega), \tag{44}$$

where

$$G_S(\omega) = 1 - A + A(1 - C^2)/[1 - 2C\cos(2\pi\omega) + C^2], \tag{45}$$

and

$$A = \eta f_S \mathrm{Corr}(T_W, T_S)/\alpha C. \tag{46}$$

When $\eta = 0$ successive summers are uncorrelated and $P_S(\omega) = \sigma_{TS}^2$.

Figure 17 shows $P_S(\omega)$ for standard values (thin line) and for some parameter variations (cf. the winter spectra in Fig. 11). For standard values the spectrum is weakly red. Increasing the winter damping rate κ_W to $40\mathrm{Wm}^{-2}\mathrm{K}^{-1}$ reduces the winter temperature anomalies that persist into summer, flattening the spectrum (Fig. 17a). Increasing the summer damping rate κ_S to $40\mathrm{Wm}^{-2}\mathrm{K}^{-1}$ reduces the summer variance considerably (Fig. 17b). Doubling the winter depth h_W increases the power at interannual scales and reduces it at decadal scales (Fig. 17c). Doubling the winter forcing σ_{QW} increases the power slightly, more so at low frequencies (Fig. 17d).

9. Discussion

In the mid to high latitude oceans the seasonal variability of SST is influenced by the re-emergence process, by which upper ocean temperature anomalies sequestered beneath the shallow summer mixed layer are mixed into the deeper

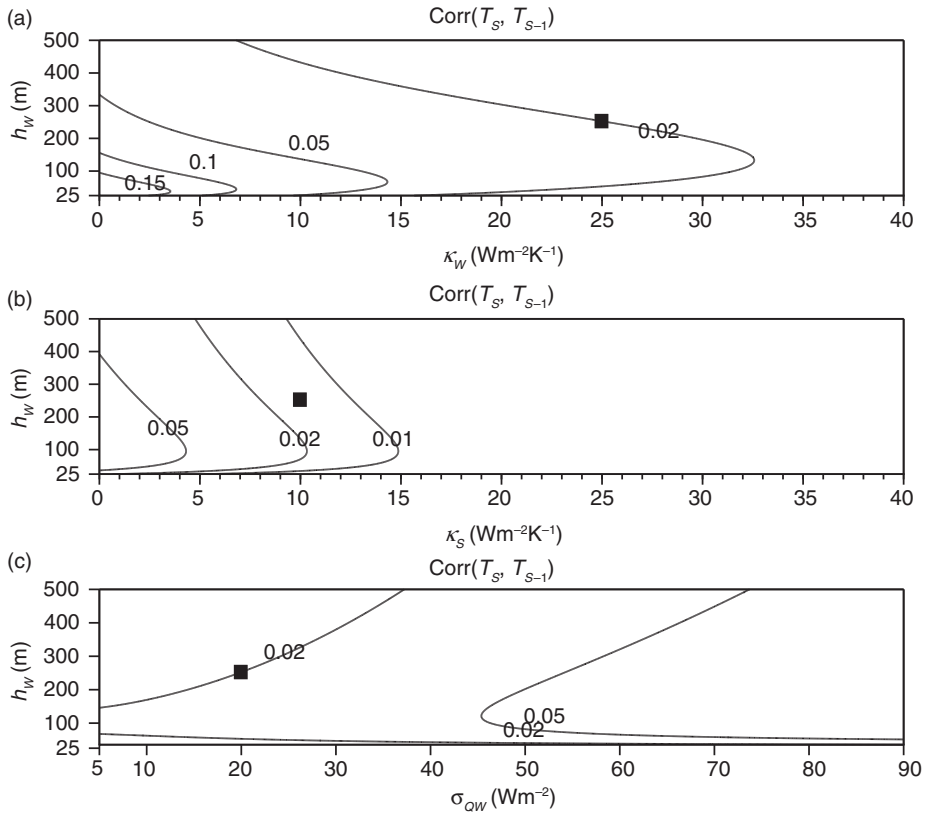

Fig. 16. Summer-to-summer correlation Corr(T_S,T_{S-1}). (a) dependence on winter damping rate κ_W and depth h_W, (b) dependence on summer damping rate κ_S and winter depth h_W, (c) dependence on winter forcing σ_{QW} and depth h_W.

winter mixed layer. The extent of this influence depends on factors such as the relative depth of the mixed layers and the strength of surface heat fluxes. The purpose of this article is to describe a novel idealised model aimed at exploring the effects of several factors. The main simplifying assumptions are the restriction to two seasons in the year, fixed mixed layer depths in the 'summer' and 'winter' seasons, and surface fluxes with a fixed forcing component within each season (varying stochastically from season to season) and a linear damping component. The strength of the model is that its simplicity allows analytic expressions to be derived for statistical properties such as seasonal temperature variance and season-to-season correlations. The main variables are end-of-season temperature anomalies: at the expense of extra algebraic complexity, the model could also be written in terms of seasonal-average anomalies, with similar qualitative behaviour.

The formulation of the model (Section 2) includes two 'process flags'. The 're-emergence' flag γ controls the subsurface temperature anomaly that influences the following winter, and the 'persistence' flag η controls the winter temperature anomaly that influences the following summer. These flags allow the roles of the respective processes to be traced in the derivation and interpretation of the analytic expressions. The parameters in the model are the summer and winter mixed layer depths h_S and h_W, the summer and winter damping rates κ_S and κ_W, the standard deviations of the summer and winter forcing σ_{QS} and σ_{QW}.

A set of standard values for the model parameters is provided in Table 1, representative of a mid-latitude ocean location, and select corresponding statistical values can be found in Table 2. The effects of parameter variations are described in Sections 3–8.

As derived in Section 2 and the Appendix, a particularly simple expression is obtained for the correlation C of end-of-winter temperature anomalies from one winter to the next:

$$C = f_W[r\eta f_S + \gamma(1-r)], \tag{47}$$

where r is the depth ratio h_S/h_W, and f_W and f_S are expressions for the attenuation of anomalies through winter and summer, respectively, through damping effects (tending to zero for strong damping and 1 for weak damping). Note that C does not depend on the forcing terms. When flags η and γ are zero the anomalies each season are independent of those preceding, and $C=0$. When the flag γ is zero and

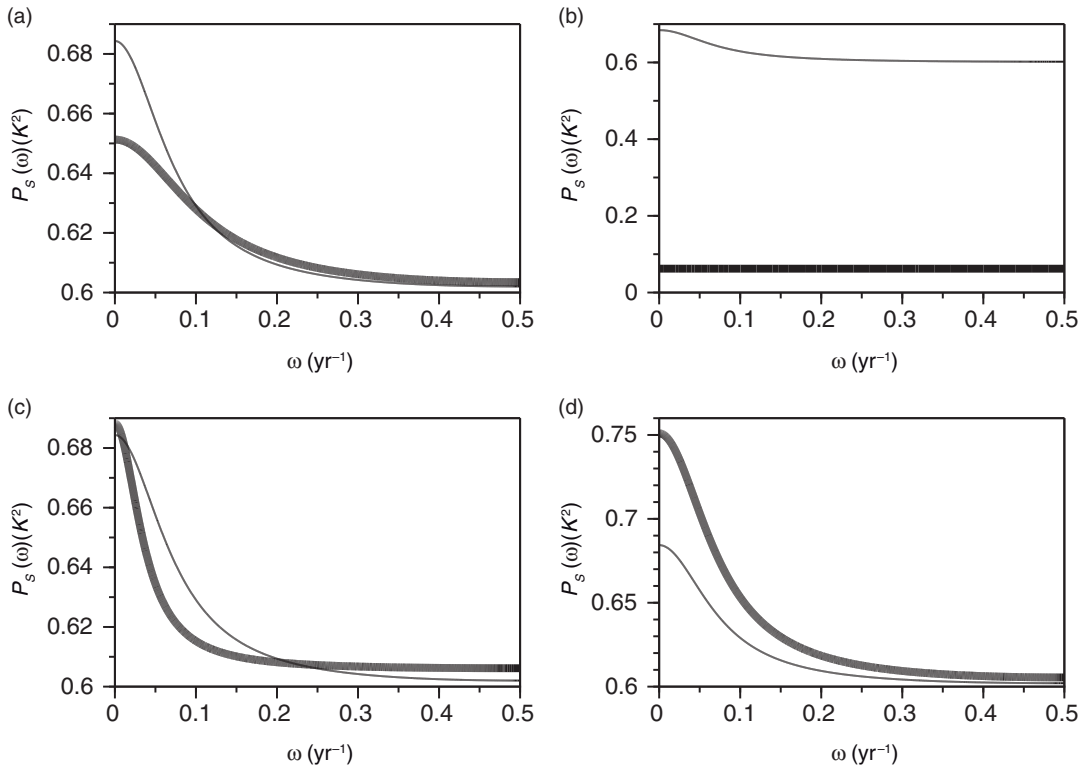

Fig. 17. Power spectrum $P_S(\omega)$ of summer temperature anomalies. In each case the thin line is $P_S(\omega)$ for standard values, the thick line for parameter variations. (a) winter damping k_W increased to 40 $Wm^{-2}K^{-1}$, (b) summer damping κ_S increased to 40 $Wm^{-2}K^{-1}$, (c) winter depth h_W doubled to 500 m, (d) winter random forcing σ_{QW} doubled to 40 Wm^{-2}.

η is unity then re-emergence is 'off', but C is positive due to persistence effects. When γ is also unity then re-emergence increases C. It can be deduced that the re-emergence contribution to C is larger when $h_W > (1+f_S)h_S$, which is always true when $h_W > 2h_S$. The dependence of C on damping and on h_W is discussed in Section 3, with the tendency for larger C with larger h_W being the dominant feature (see Fig. 3). Stronger winter damping and stronger re-emergence through deeper h_W have competing effects, manifest in the parameter combination rf_W illustrated in Fig. 4.

The equation for C also leads to a simple analytic expression for multi-year lag correlations and hence for the winter power spectrum, as described in Section 5. When $C=0$ ($\eta=\gamma=0$) the spectrum is white, with amplitude depending on a combination of the winter and summer forcing. For standard parameter values, activating persistence ($\eta=1$) has little effect, producing a slightly red spectrum, whereas activating re-emergence ($\gamma=1$) has a large effect, as shown in Fig. 10. Some effects of parameter variations on the winter spectrum are illustrated in Fig. 11.

The winter variance and its parameter dependence are discussed in Section 4. The variance decreases as h_W increases, because winter surface forcing is spread over a large depth and resulting anomalies are smaller, and as damping increases. It can be regarded as having random and predictable components, with end-of-winter temperature anomaly as the predictor for the next winter and C^2 as a measure of the predictable fraction. Re-emergence is the dominant process contributing to predictability, unless there is little difference between winter and summer depths. The amplitude of the predictable variance does not have a simple dependence on h_W: there is an optimal depth, because increasing h_W increases the influence of re-emergence but reduces the variance size.

Summer temperature variance and summer-to-winter correlations Corr(T_W, T_S) are described in Section 6. The ratio of summer to winter variance plays a role in the correlation. The ratio is increased by increasing h_W (because winter variance is reduced), but decreased by re-emergence. The summer-to-winter correlation contains a contribution from conditions in the previous winter, because through persistence and re-emergence those conditions influence both following summer and winter conditions. Thus Corr (T_W, T_S) is not just a measure of direct summer influence on the following winter, but contains an indirect component, as illustrated in Fig. 14. The implications of this for defining a measure of the re-emergence signal in terms of

winter-to-winter and summer-to-winter correlations are discussed in Section 7. Although season-to-season temperature correlations are relatively easy to estimate from temperature observations, some care is needed in interpreting the results.

To complete the description of the analytic properties of the simple two-season model, the summer-to-summer correlations and summer power spectrum are described in Section 8. The summer spectrum is relatively insensitive to parameter variations, with the exception of varying the summer forcing by which it is largely determined.

The model, however, neglects several important factors. As shown by Deser et al. (2003) and Frankignoul (1985), interannual mixed layer depth variability alters the entrainment rate, which influences the persistence of SST anomalies and the effects of re-emergence. Convective instability, which occurs when the temperature anomaly in the winter mixed layer is colder than that which resides just below the mixed layer can alter the upper ocean thermal structure, and subsequently the mixed layer depth. In the two-season model, entrainment occurs each year at the same depth. Similarly, the temperature anomaly at the start of winter can alter the mixed layer depth in the following winter. Interannual variability in the atmospheric damping may also impact re-emergence. Sura et al. (2006) showed that extending the model of Frankignoul and Hasselmann (1977) to include anomalous atmospheric feedback introduces an extra multiplicative noise term, which significantly enhances the overall stochastic forcing and produces a non-Gaussian probability density function of the winter SST similar to that which is found in observations. In the two-season model, the probability density function of the winter temperature is Gaussian. There are also vertical processes such as those associated with permanent thermocline variations induced by the first mode baroclinic Rossby wave (Zhang and Wu, 2010; Schneider and Miller, 2001); strong subduction (De Coëtlogon and Frankignoul, 2003); and non-local effects such as horizontal advection (Jin, 1997; Ostrovskii and Piterbarg, 2000) and remote ENSO forcing (Park et al., 2006) that influence mid-latitude temperature variability. The two-season model could be extended to include these factors and their effect together with re-emergence on mixed layer temperature investigated.

To summarise, the two-season approach provides a simple model of the effects of persistence and re-emergence, with parameters for layer depths, damping and forcing, in a stochastic forcing framework. The simplicity allows explicit analytic expressions to be obtained for the key properties of variance and correlation and power spectrum. Work is in progress on investigating the key results regarding for example temperature variance as a function of summer to winter mixed layer depth ratio, using ocean analysis datasets.

10. Acknowledgements

Part of this work was carried out while Peter Kowalski was at University College London, supported by a Co-operative Award in Science and Engineering studentship from the Engineering and Physical Sciences Research Council. Michael Davey was partly supported by the Joint UK DECC/Defra Met Office Hadley Centre Climate Programme (GA01101).

11. Appendix: Derivation of the analytic expressions

A.1. Notation

Let $<x>$ denote the average of variable x_i over a large sample. (Large means many times the damping timescale, which for standard parameters corresponds to several decades.) As $<Q_S> = <Q_W> = 0$ in the damped two-season system, it follows from averaging the regression relations that $<T_S> = <T_W> = 0$. The summer and winter temperature anomaly variances are $\sigma_{TS}^2 = <T_S^2>$ and $\sigma_{TW}^2 = <T_W^2>$. The covariance between winter and previous summer is denoted

$$\mathrm{Cov}(T_W, T_S) = <T_W T_S>, \tag{A1}$$

and the lagged covariance between winter and winter j years previously is denoted

$$\mathrm{Cov}(T_W, T_{W-j}) = <T_W T_{W-j}>. \tag{A2}$$

The correlation is denoted, for example,

$$\mathrm{Corr}(T_W, T_S) = \mathrm{Cov}(T_W, T_S)/\sigma_{TW}\sigma_{TS}. \tag{A3}$$

Note that as the stochastic atmospheric forcing Q is independent of preceding temperatures then, for example,

$$\mathrm{Cov}(Q_S, T_{W-1}) = 0,\ \mathrm{Cov}(Q_W, T_S) = 0. \tag{A4}$$

A.2. Correlations and variances

A.2.1. Winter-to-winter correlation and winter temperature variance

From the winter-to-winter autoregression, eq. (17), it is straightforward to deduce that

$$\mathrm{Corr}(T_W, T_{W-1}) = C, \tag{A5}$$

and

$$\sigma_{TW}^2 = \sigma_R^2/(1 - C^2), \tag{A6}$$

where

$$\sigma_R^2 = r^2 f_W^2 (1 - f_S)^2 (\sigma_{QS}^2/\kappa_S^2) + (1 - f_W)^2 (\sigma_{QW}^2/\kappa_W^2) \tag{A7}$$

and C is defined in eq. (18).

A.2.2. Summer temperature variance

Multiplying eq. (12) by T_{Si} and then taking the ensemble average yields

$$\sigma_{TS}^2 = f_S\eta \mathrm{Cov}(T_S, T_{W-1}) + (1-f_S)\mathrm{Cov}(T_S, Q_S)/\kappa_S. \quad \text{(A8)}$$

Multiplying eq. (12) by T_{Wi-1}, and using eq. (A4) gives

$$\mathrm{Cov}(T_S, T_{W-1}) = f_S\eta\sigma_{TW}^2. \quad \text{(A9)}$$

Similarly, it can be shown using eq. (16) that

$$\mathrm{Cov}(T_S, Q_S) = (1-f_S)\sigma_{QS}^2/\kappa_S. \quad \text{(A10)}$$

Substituting eq. (A10) and (A9) in eq. (A8) yields

$$\sigma_{TS}^2 = f_S^2\eta^2\sigma_{TW}^2 + (1-f_S)^2\sigma_{QS}^2/\kappa_S^2. \quad \text{(A11)}$$

A.2.3. Summer-to-winter correlation

Multiplying eq. (17) by T_{Si} and using eqs. (A9) and (A10), leads to

$$\mathrm{Cov}(T_W, T_S) = Cf_S\eta\sigma_{TW}^2 + f_W r(1-f_S)^2\sigma_{QS}^2/\kappa_S^2. \quad \text{(A12)}$$

Using eq. (A11) and the definition of C in eq. (18), this can be written as

$$\mathrm{Cov}(T_W, T_S) = \eta f_S f_W\gamma(1-r)\sigma_{TW}^2 + f_W r\sigma_{TS}^2. \quad \text{(A13)}$$

Dividing eq. (A13) by $\sigma_{TS}\,\sigma_{TW}$ leads to an expression for the summer-to-winter correlation:

$$\mathrm{Corr}(T_W, T_S) = f_W[r\alpha + \gamma\eta(1-r)f_S/\alpha], \quad \text{(A14)}$$

where $\alpha = \sigma_{TS}/\sigma_{TW}$ is the ratio of summer to winter standard deviation, which is known from eqs. (A6) and (A11).

A.2.4. Summer-to-summer covariance

Multiplying eq. (12) by T_{Si-1}, and using $< Q_S T_{S-1} >= 0$ and $< T_{W-1}T_{S-1} >=< T_W T_S >$, leads to

$$\mathrm{Cov}(T_S, T_{S-1}) = f_S\eta\mathrm{Cov}(T_W, T_S), \quad \text{(A15)}$$

with $\mathrm{Cov}(T_W, T_S)$ known from eq. (A13). Similarly,

$$\mathrm{Cov}(T_S, T_{S-j}) = f_S\eta\mathrm{Cov}(T_W, T_{S-(j-1)}). \quad \text{(A16)}$$

Multiplying eq. (17) by T_{Si-1} and averaging, again using $< T_{W-1}T_{S-1} >=< T_W T_S >$leads to

$$\mathrm{Cov}(T_W, T_{S-1}) = C\mathrm{Cov}(T_W, T_S). \quad \text{(A17)}$$

Similarly,

$$\mathrm{Cov}(T_W, T_{S-k}) = C^k\mathrm{Cov}(T_W, T_S), \quad \text{(A18)}$$

which can be substituted in eq. (A16) to give

$$\mathrm{Cov}(T_S, T_{S-j}) = \eta f_S C^{j-1}\mathrm{Cov}(T_W, T_S). \quad \text{(A19)}$$

It is convenient to write eq. (A19) as

$$\mathrm{Cov}(T_S, T_{S-j}) = A\sigma_{TS}^2 C^j, \quad \text{(A20)}$$

where

$$A = \eta f_S\mathrm{Cov}(T_W, T_S)/\sigma_{TS}^2 C. \quad \text{(A21)}$$

Note that eq. (A20) is only valid when $j \geq 1$. When $j = 0$, $\mathrm{Cov}(T_S, T_S) = \sigma_{TS}^2$ as defined in eq. (A11).

A.2.5. Summer-to-summer correlation

Using eqs. (A14), (A15), and (A20) it is straightforward to show that the summer-to-preceding summer correlation is

$$\begin{aligned}\mathrm{Corr}(T_S, T_{S-1}) &= AC \\ &= \eta f_S\mathrm{Corr}(T_W, T_S)/\alpha \\ &= f_W f_S\eta[r + \gamma\eta f_S(1-r)/\alpha^2].\end{aligned} \quad \text{(A22)}$$

A.3. Power spectra

A.3.1. Winter temperature

The power spectrum of the winter temperature, $P_W(\omega)$, can be found by performing the discrete Fourier transform of the covariance function $\mathrm{Cov}(T_W, T_{W-j})$:

$$P_W(\omega) = \sum_{j=-\infty}^{j=\infty}\mathrm{Cov}(T_W, T_{W-j})e^{-i2\pi\omega j}, \quad \text{(A23)}$$

where $\omega \in [0, 0.5]$, and the Nyquist frequency $\omega = 0.5$ corresponds to a period of 2 years in our model. From the winter-to-winter relations,

$$\mathrm{Cov}(T_W, T_{W-j}) = C^j\sigma_{TW}^2, \quad \text{(A24)}$$

and it follows that

$$P_W(\omega) = \sigma_R^2 G_W(\omega), \quad \text{(A25)}$$

where the spectral shape is

$$G_W(\omega) = 1/[1 - 2C\cos(2\pi\omega) + C^2]. \quad \text{(A26)}$$

Note that $G_W(0) = 1/(1-C)^2 \geq 1$, and $G_W(0.5) = 1/(1+C)^2 \leq 1$.

A.3.2. Summer temperature

Similarly the power spectrum $P_S(\omega)$ of the summer temperature can be found from

$$P_S(\omega) = \sum_{j=-\infty}^{j=\infty}\mathrm{Cov}(T_S, T_{S-j})e^{-i2\pi\omega j}, \quad \text{(A27)}$$

which can be written as

$$P_S(\omega) = \sigma_{TS}^2 + 2\sum_{j=1}^{j=\infty} \mathrm{Cov}(T_S, T_{S-j})\cos(2\pi\omega j), \qquad \text{(A28)}$$

since $\mathrm{Cov}(T_S,T_{S-j})$ is an even function of j. Substituting eq. (A20) in (A27) yields

$$P_S(\omega) = \sigma_{TS}^2[1 + 2A\sum_{j=1}^{j=\infty} C^j \cos(2\pi\omega j)], \qquad \text{(A29)}$$

which is

$$P_S(\omega) = \sigma_{TS}^2[1 + A\sum_{j=1}^{j=\infty} (Ce^{i2\pi\omega})^j + (Ce^{-i2\pi\omega})^j]. \qquad \text{(A30)}$$

It straightforward to show that

$$P_S(\omega) = \sigma_{TS}^2 G_S(\omega), \qquad \text{(A31)}$$

where

$$G_S(\omega) = 1 - A + A(1 - C^2)G_W(\omega). \qquad \text{(A32)}$$

References

Alexander, M. A. and Deser, C. 1995. A mechanism for the recurrence of wintertime midlatitude anomalies. *J. Phys. Oceanogr.* **25**, 122–137.

Alexander, M. A., Deser, C. and Timlin, M. S. 1999. The reemergence of SST anomalies in the North Pacific Ocean. *J. Clim.* **12**, 2419–2433.

Ciasto, L. M., Alexander, M. A., Deser, C. and England, M. H. 2010. On the persistence of cold-season SST anomalies associated with the Annular Modes. *J. Clim.* **24**, 2500–2515.

Ciasto, L. M. and Thompson, D. W. J. 2009. Observational evidence of reemergence in the extratropical southern hemisphere. *J. Clim.* **22**, 1446–1453.

De Coëtlogon, G. and Frankignoul, C. 2003. The persistence of winter sea surface temperature in the North Atlantic. *J. Clim.* **16**, 1364–1377.

Deser, C., Alexander, M. A. and Timlin, M. 2003. Understanding the persistence of sea surface temperature anomalies in midlatitudes. *J. Clim.* **16**, 57–72.

Folland, C. K., Scaife, A. A., Lindesay, J. and Stephenson, D. B. 2012. How potentially predictable is northern European winter climate a season ahead? *Int. J. Climatol.* **32**(6), 801–808. DOI: http://dx.doi.org/10.1002/joc.2314

Frankignoul, C. 1985. Sea surface temperature anomalies, planetary waves and air-sea feedback in the middle latitudes. *Rev. Geophys.* **23**, 357–390.

Frankignoul, C., Czaja, A. and L'Heveder, B. 1998. Air-sea feedback in the North Atlantic and surface boundary conditions for ocean models. *J. Clim.* **11**, 2310–2324.

Frankignoul, C. and Hasselmann, K. 1977. Stochastic climate models, Part 2. Application to sea-surface temperature anomalies and thermocline variability. *Tellus.* **29**(4), 289–305.

Hanawa, K. and Sugimoto, S. 2004. Reemergence areas of winter sea surface temperature anomalies in the world's oceans. *Geophys. Res. Lett.* **31**(10), L10303. DOI: http://dx.doi.org/10.1029/2004GL019904

Jin, F. 1997. A theory of interdecadal climate variability of the North Pacific ocean-atmospheric system. *J. Clim.* **10**, 1821–1835.

Namias, J. and Born, R. M. 1970. Temporal coherence in the North Pacific sea-surface temperature patterns. *J. Geophys. Res.* **75**, 5952–5955.

Namias, J. and Born, R. M. 1974. Further studies of temporal coherence in North Pacific sea surface temperatures. *J. Geophys. Res.* **79**, 797–798.

Ostrovskii, A. and Piterbarg, L. 2000. Inversion of upper ocean temperature time series for entrainment, advection and diffusivity. *J. Phys. Oceanogr.* **30**, 201–214.

Park, S., Alexander, M. A. and Deser, C. 2006. The impact of cloud radiative feedback, remote ENSO forcing, and entrainment on the persistence of north pacific sea surface temperature anomalies. *J. Clim.* **19**, 6243–6261.

Rodwell, M. J. and Folland, C. K. 2002. Atlantic air-sea interaction and seasonal predictability. *Q. J. Roy. Meteorol. Soc.* **128**, 1413–1443.

Schneider, N. and Cornuelle, B. D. 2005. The forcing of the Pacific Decadal Oscillation. *J. Clim.* **18**, 4355–4373.

Schneider, N. and Miller, A. J. 2001. Predicting western North Pacific Ocean climate. *J. Clim.* **14**, 3997–4002.

Sura, P., Newman, M. and Alexander, M. A. 2006. Daily to decadal sea surface temperature anomalies driven by state dependent stochastic heat fluxes. *J. Phys. Oceanogr.* **36**, 1940–1958.

Taws, S. L., Marsh, R., Wells, N. and Hirshi, J. 2011. Re-emerging ocean temperature anomalies in late-2010 associated with the repeat negative NAO. *Geophys. Res. Lett.* **38**(20), L20601. DOI: http://dx.doi.org/10.1029/2011GL048978

Timlin, M. S., Alexander, M. A. and Deser, C. 2002. On the reemergence of the North Atlantic SST anomalies. *J. Clim.* **15**, 2707–2712.

Watanabe, M. and Kimoto, M. 2000. On the persistence of decadal SST anomalies in the North Atlantic. *J. Clim.* **13**, 3017–3028.

Zhang, H. and Wu, L. 2010. Predicting North Atlantic sea surface temperature variability on the basis of the first-mode baroclinic Rossby wave model. *J. Geophys. Res.* **115**, C09030. DOI: http://dx.doi.org/10.1029/2009JC006017

Zhao, X. and Li, J. 2012. Winter-to-winter recurrence and non-winter-to-winter recurrence of SST anomalies in the central North Pacific. *J. Geophys. Res.* **117**, C05027. DOI: http://dx.doi.org/10.1029/2011JC007845